Published as: *Nat Neurosci*. 2013 July ; 16(7): 958–965.

Neural coding during active somatosensation revealed using illusory touch

Daniel H. O'Connor[1,†,*], **S. Andrew Hires**[1,*], **Zengcai V. Guo**[1], **Nuo Li**[1], **Jianing Yu**[1], **Qian-Quan Sun**[1,#], **Daniel Huber**[1,%], and **Karel Svoboda**[1]

[1]Janelia Farm Research Campus, HHMI, Ashburn VA 20147

Abstract

Active sensation requires the convergence of external stimuli with representations of body movements. We used mouse behavior, electrophysiology and optogenetics to dissect the temporal interactions between whisker movement, neural activity, and sensation of touch. We photostimulated layer 4 activity in single barrels in closed-loop with whisking. Mimicking touch-related neural activity caused illusory perception of an object at a particular location, but scrambling the timing of spikes over one whisking cycle (tens of milliseconds) did not abolish the illusion, indicating that knowledge of instantaneous whisker position is unnecessary for discriminating object locations. Illusions were induced only during bouts of directed whisking, when mice expected touch, and in the relevant barrel. Reducing activity biased behavior consistent with a spike count code for object detection at a particular location. Our results show that mice integrate coding of touch with movement over timescales of a whisking bout to produce perception of active touch.

Introduction

Animals explore the world by moving their sensors across objects and scenes of interest. The brain therefore must interpret sensory input in the context of sensor movement. The relative timing of neural signals representing movement (efference or re-afference) and sensation (exafference) is critical for sensorimotor integration. For example, a tickling stimulus, when self-applied, fails to evoke the perception of tickling; however, when the same stimulus arrives out of phase with self-movement, tickling is perceived [1].

Correspondence and requests for materials should be addressed to svobodak@janelia.hhmi.org.
[†]Current address: The Solomon H. Snyder Department of Neuroscience & Brain Science Institute, The Johns Hopkins University School of Medicine, Baltimore, MD 21205
[#]Current address: Department of Zoology and Physiology, University of Wyoming, Laramie, Wyoming 82071
[%]Current address: Department of Basic Neurosciences, University of Geneva, CH-1211 Geneva, Switzerland.
[*]These authors contributed equally to this work.

Supplementary Information is linked to the online version of the paper at www.nature.com/nature.

Author Contributions.

DHO, SAH, ZVG, NL, JY and QQS performed experiments. DH, ZG and NL developed the symmetric response task paradigm. DHO, SAH and KS planned the project. DHO, SAH, ZVG, NL and KS analyzed the data. DHO, SAH and KS wrote the paper with comments from other authors.

The rodent vibrissal system is advantageous for studying the mechanisms underlying sensorimotor integration during active sensation, because movement and sensory input can be tracked with high precision [2–7]. Rodents explore the tactile world by moving their mystacial vibrissae (whiskers) rhythmically [2,3,6], in directed bouts of whisking lasting several whisking cycles (approximately 50 ms per cycle in mice) [6,8]. Whisking thus involves vibrissa movement over multiple time scales: the single whisking cycle and directed whisking bouts lasting hundreds of milliseconds.

Head-fixed mice can discriminate two object locations in the azimuthal plane, even with a single whisker [6]. Under these conditions mice have to interpret whisker touch in the context of whisker movement to detect objects at particular locations [8,9]. Rodents solve this task using a directed whisking strategy, favoring one of the two object locations [2,6,9]. At least two algorithms, relying on distinct tactile cues, could underlie this form of object location discrimination. First, mice could extract object location as the whisker position at the moment of touch [10]. This strategy relies on a high-fidelity, cycle-by-cycle representation of whisker position and millisecond timescale (i.e. much shorter than a single whisking cycle) coding of touch, but does not require coding of the forces acting on the whisker. Second, mice could decode the patterns and amplitudes of touch-related forces, which depend on the location of the object [5,7]. This strategy relies on knowledge of the range and direction of whisking during a bout, but does not make reference to instantaneous whisker position and may not require millisecond timescale precision in the coding of touch.

The vibrissal somatosensory cortex (vS1) is critical for detecting an object at a particular location [6,11]. Contact between whisker and object evokes phasic spikes in all layers of vS1 [12,13].

Anatomical connections between sensory and motor areas allow for interactions between whisking and touch [14]. Furthermore, vS1 is the target of efferent signals from the motor cortex [15,16], which controls task-related whisking [17], as well as reafference signals, which arise in sensory neurons and ascend via multiple thalamic nuclei into the cortex [18,19]. Whisker position is represented at the level of spikes and membrane potential in vS1 [20,21]. These observations suggest that signals associated with whisking and touch interact in vS1.

Here we probe how touch is interpreted in the context of whisker movement during a task in which mice discriminate two object locations (also referred to as 'object localization' in some previous studies [2,6,8]) using a single whisker. We focus on L4 neurons in vS1. L4 neurons in individual barrels (approximately 2000 neurons per barrel) process information from single whiskers [22–24]. L4 stellate cells receive the majority of excitatory input from sensory thalamus and additional input from other L4 stellate cells [22,25,26]. They project to L2/3 and L5 in the barrel cortex [22]. Barrels in L4 of vS1 thus form a bottleneck, linking information related to sensation with a particular whisker and cortical processing.

L4 neurons respond to whisker touch with short-latency spikes, with timing jitter on the order of a few milliseconds [23,24]. When referenced to a neural representation of the rapidly changing whisker position or whisking phase [20,21], millisecond time scale spike latency

provides information about object location [14,27]. L4 neurons also encode the strength of the interaction between whisker and object, yielding alternative cues about object location.

We used behavioral analysis, electrophysiology and optogenetics to examine how whisker movement and touch can together discriminate object location. Mice solved the task by preferentially whisking in one of two object locations, perhaps maximizing the difference in the number of touches and whisker forces between object locations [6,12]. One interpretation is that mice convert object location discrimination into a problem of detecting the object in one of the two locations [6]. To reveal the timescale of integration of L4 spikes and whisker movements, we coupled channelrhodopsin-2 (ChR2) photostimulation [28,29] in L4 neurons to whisker position with millisecond precision. Mimicking touch-evoked activity in L4 neurons was sufficient to evoke behavior consistent with illusory perception of an object in a target location, but only in the C2 representation area of vS1. Temporally precise coupling between activity and whisker movement was not required for this illusion, but photostimulated activity had to occur coincident with bouts of directed whisking to evoke illusory perception of touch with a target object. These results suggest a spike count code underlying object location discrimination within defined regions of cortical space and defined behavioral epochs lasting at least a full whisk cycle. Our experiments further illustrate the power of combining trained perceptual behaviors, neuronal recordings, and closed-loop, cell-type specific optogenetic perturbations in dissecting neural coding in complex, hierarchical circuits.

Results

Neuronal encoding of object location

We trained head-fixed mice to perform a memory-guided, whisker-based object location discrimination task with the C2 whisker (Fig. 1a, b) [6]. In each trial, a pole was moved into one of two locations arranged in the posterior-anterior direction on one side of the head. High-speed videography and automated whisker tracking allowed us to reconstruct whisker movements and detect contacts between whisker and pole with millisecond precision [4,6]. Mice reported their decision about object location with licking or not licking. All experiments were performed in trained mice (n = 33 mice, fraction of trials correct: 0.75 ± 0.08, mean ± STD; **Methods**).

Mice typically began to whisk before the pole came within reach and continued throughout the 'exploration window' (see **Methods**; the epoch between the trial start cues and the typical response; duration 1.20 ± 0.16 seconds). Mice whisked with large amplitudes in short bouts (bout duration, 0.5–2 s; peak-to-peak amplitude, 44 ± 16 degrees; frequency, 17 Hz). Over the time-course of learning, mice adjusted the setpoint of whisking [15] during the exploration window to align with one of the pole locations [6] (Fig. 1c, d), a general feature of the whisking strategies in these types of tasks [2,9,16,17,30]. The region in space traversed by the whisker, the 'azimuthal region of interest' (θ_{ROI}), was thus approximately centered on this pole location (Fig. 1c; sFig. 1). For most experiments (except for the experiments in sFig. 5) θ_{ROI} corresponded to the posterior pole location. We refer to trials with the pole near the center of the θ_{ROI} as 'YES trials' (correct response, 'yes') and trials with the other pole location as 'NO trials' (correct response, 'no'). On individual YES trials the whisker

typically touched the pole multiple times (mean, 4.09), whereas contacts were less frequent on NO trials (mean, 1.15) (Fig. 1e).

Based on loose seal, cell-attached recordings, which sample neurons independent of their activity patterns, we estimate that 78 % of L4 neurons within and near the active barrel are modulated by touch[12]. We recorded from additional L4 neurons in and around the C2 barrel (< 250 μm from the C2 center) during object localization with a single whisker (cell-attached, n=10; silicon probe, n=21). Whisker position and contacts were tracked with 1 millisecond precision (Fig. 1d). Neurons rapidly excited by touch had short latencies (threshold latency 8.7 ms ± 3.0 ms, n = 13) and small jitter across trials (5.2 ± 1.3 ms first spike STD) (Fig. 2a, b).

Object location discrimination in the azimuthal plane requires the integration of information about whisker position and whisker touch [98]. Two different types of behavioral strategies could underlie object location discrimination. First, mice could extract the position of the whisker at the time of contact (Fig. 3a). This is plausible because barrel cortex contains a neural representation of cycle-by-cycle whisker movement [20,21,27], and precisely timed contact signals (Fig. 2a, b). Second, the whisker interacts differentially with objects in different locations within the azimuthal region of interest (e.g. relatively strongly in the YES location). Object location within the θ_{ROI} can thus be derived by measuring contact forces, without reference to rapid whisker movement. The directed whisking pattern adopted by mice in our task, where θ_{ROI} is centered on one of the pole locations, is consistent with both strategies (Fig. 1c–e; Fig. 3a).

These two behavioral strategies map onto distinct neural codes. Because of the small latency jitter (Fig. 2a, b), the spike-triggered position of the whisker (azimuthal angle, θ at touch) differed for trials with different object locations (Fig. 3b). The timing of the synchronous activity seen in L4 referenced to rapid whisker movement [20,21,27] (spike timing) codes for whisker position at touch and thus for object location (Fig. 3a, b). However, because the whisker interacts more often, and likely more strongly [6], with the YES stimulus compared to the NO stimulus (Fig. 1c–e; Fig. 3a), the number of spikes (spike count) also differed across object locations (Fig. 3c).

We compared the ability of these two neural codes to discriminate object location and behavioral choice by applying a linear classifier to each L4 neuron (n=31). Across the population, object location was discriminated equally well using information about spike timing and spike count (Fig. 3d). Similarly, the mouse's behavioral choice (yes/no) could be discriminated using both coding schemes, although spike count performed slightly better compared to spike-triggered θ ($p = 0.0085$) (Fig. 3e). To establish a causal link between these two aspects of L4 activity and perception, we independently manipulated the timing and rate of L4 activity using optogenetics.

Closed-loop photostimulation of L4 causes illusory touch

Manipulations of activity during behavior can reveal the spike train features that are decoded to drive decisions [31,32]. Manipulations in closed-loop with movement are necessary to establish causality between behavior and spike-timing relative to movement. We thus

developed methods to control activity in space and time, producing precise synthetic spike trains during behavior (Fig. 1a, 4a).

To target L4 neurons in a specific barrel for photostimulation we used transgenic mice expressing Cre recombinase selectively in L4 neurons [25,33,34] together with adeno-associated virus (AAV) expressing ChR2 [35] in a Cre-dependent manner [36]. Virus was injected into the C2 column, guided by intrinsic signal imaging [37], resulting in ChR2 expression in L4 neurons in the vicinity of the C2 column (Fig. 4a; sFig 2).

We recorded light-evoked spikes from neurons in the C2 barrel column in awake mice using cell-attached recordings [12] (Fig. 4b–d). Brief light pulses (typically 1 ms; wavelength, 473 nm; intensity range, 5–32 mW/mm^2; Methods) [38] evoked spikes with short latencies (2.3 ± 1.2 ms, mean ± std, n = 12), presumably directly triggered by light-gated current, in a subpopulation (50 %; 12/24) of L4 neurons (Fig. 4b–d). Longer latency spikes were detected in L2/3 (3.5 ± 1.1 ms, n = 9, $p < 0.05$; one-tailed permutation test) and L5 (5.5 ± 4.0 ms, n = 23, $p < 0.01$; one-tailed permutation test) cells, consistent with synaptic activation of these neurons [22] (Fig. 4c). Overall, single photostimuli and whisker contacts evoked similar activity across populations of L4 neurons (Fig. 4e).

We next asked if photostimulating L4 neurons can evoke illusory sensation of touch and perception of object location. We positioned a virtual pole, created by the beam of an infrared laser, right next to one of the pole positions along the whisker (Fig. 1a, 5a). A photodiode and a real-time computer system detected the whisker crossing the virtual pole and also controlled the photostimulus with submillisecond precision. This temporal precision is necessary because mouse whiskers move with azimuthal speeds of up to five degrees per millisecond [6]. The closed-loop system allowed us to mimic touch-evoked activity in L4 (duration of evoked population activity, FWHM; photostimulation, 4.73 ms; touch, 7.72 ms; Fig. 4e).

All behavioral experiments were performed on mice trained only on the object location discrimination task. On a subset of trials (25 %) photostimuli were delivered coupled to whisker crossings (Fig. 5a–c). Each trial type (YES, NO) was photostimulated with equal probability; only the pole location, but not photostimulation, predicted reward. A single light pulse (typically 1 ms, 41 mW/mm^2) was triggered per whisker crossing, producing approximately one action potential, similar to activity evoked by single touches (sFig. 3; Fig. 4e) [38]. Mice 'palpated' the virtual pole multiple times per trial, triggering a corresponding number of photostimuli (Fig. 5b; sFig. 4). Based on the touch-to-spike latencies measured during discrimination behavior (~ 9 ms; Fig. 4d; sFigs. 3, 4), we chose 5 milliseconds as the delay between whisker crossing and photostimulation. Similar to actual contacts, whisker crossings are thus followed by synchronized activity in subpopulations of L4 neurons in the relevant barrel (total delay of whisker crossing to evoked spike, ~ 9 ms, (Fig. 4d; Fig. 4e).

To determine if photostimulation of L4 neurons is sufficient to evoke illusory perception of object location we focused our analysis on NO trials, with the virtual pole centered in the θ_{ROI} and the actual pole towards the edge of the θ_{ROI} (Fig. 5a). With photostimulation mice

were more likely to respond 'yes', consistent with photostimulation evoking a sensation of 'illusory touch' at the YES location. We used the difference in 'yes' response probability between stimulated and non-stimulated NO trials to quantify illusory touch (Fooling Index, 0.21 ± 0.06, mean ± STD, n=6 mice; $p < 0.001$, two-tailed t-test) (Fig. 5d, e). Responses consistent with illusory touch in the YES location were evoked in about half of the stimulated NO trials, starting in the first behavioral session with photostimulation ($p = 0.008$, permutation test) (Fig. 5e). Laser light itself, without triggering L4 activity, had no effect (Fooling Index, 0.002 ± 0.051, $p = 0.93$, n=5 mice) (Fig. 5f; sFig. 7f). Illusory touch was also evoked with the YES and NO locations reversed (NO posterior; YES, anterior; sFig. 5).

We next performed experiments to determine if mice read out L4 activity in general, or only respond to activity in the somatotopic location corresponding to the spared whisker (i.e. C2). We introduced ChR2 into the E3 barrel, 750 micrometers from C2. As before, these mice were trained to discriminate object locations with the C2 whisker. Stimulation of the E3 barrel did not produce illusory touch (Fooling Index, 0.004 ± 0.034, $p = 0.87$, n=4 mice) (Fig. 5g). These experiments show that mice attend to cortical activity in a particular somatotopic location, defined by perceptual learning, and ignore activity in other locations. In addition, these experiments rule out non-specific effects of light-evoked activity.

We next addressed the possibility that photostimulation of neurons in the attended somatotopic location could somehow trigger 'yes' responses (i.e. licking), independent of perception of object location. We trained mice in a task in which both object locations were indicated by licking, but at one of two lickports ('symmetric response task', Fig. 5h). 'Yes' responses corresponded to licking to the right, and 'no' responses to licking to the left. Under these conditions mice again focused their whisking on one of the pole locations (Fig. 5h; sFig. 6). The whisking strategy employed by the mice is thus related to object location discrimination, and is independent of how reward is coupled to the stimulus. As before, we introduced the virtual pole within the θ_{ROI} and analyzed responses on NO trials. Mice were more likely to respond 'yes' after photostimulation (Fig. 5h). These experiments show that precisely timed photostimulation, in neuronal ensembles defined by infection with AAV virus and Cre expression, can evoke illusory perception of object location. Moreover, a trial-by-trial analysis of behavioral responses, photostimulation, and whisker-pole contact indicated that photostimulation and real touch showed similar patterns of behavioral saturation, partly occluded one another, and were largely interchangeable (sFig. 7).

Precisely timed spikes are not required

We tested if illusory touch in the YES location required precise spike timing with respect to a whisker position signal representing cycle-by-cycle whisker movement. We varied the photostimulation latency (time between virtual pole crossing and photostimulation, Δt) over a range from 0 to 50 milliseconds (Fig. 6a; 'delayed' light). At $\Delta t = 0$ ms, light-evoked spikes occur before touch-evoked activity would have occurred. At $\Delta t \geq 20$ ms, whisker position at the time of photostimulation spanned the entire θ_{ROI} (sFig. 8a). This is because the retraction phase of whisking is extremely fast (< 20 ms; Fig. 6a, bottom). There was no relationship between photostimulation latencies and fooling (Fig. 6b; $p = 0.73$, ANOVA).

This demonstrates that illusory touch in the YES location can be induced over a wide range of latencies, corresponding to whisker positions throughout the θ_{ROI}.

In these experiments all stimuli were delayed as a block, and the pattern of activity (i.e. the sequence of inter-photostimulation intervals) was thus preserved. In a separate set of experiments we applied photostimulus trains that were statistically identical, but did not correspond to the pattern of whisker crossings within a trial ('shuffled light' trials; the pattern of photostimuli matched the pattern of virtual pole crossings from 5 trials ago). Mice were still fooled, although the effect was smaller than for the standard experiment (sFig. 8b, c; Fooling Index 0.12 vs. 0.20; 1 of 3 mice $p < 0.05$, two-tailed permutation test). These experiments show that illusory touch does not require L4 activity to match the precise pattern of virtual pole crossings. We further examined whether illusory touch in the YES location varied with the position of the whisker at the time of initial photostimulation. We did not detect a position dependence (Fig. 6c, $p = 0.84$, ANOVA). Together these experiments indicate that perception of object location in our task does not depend on L4 activity being interpreted with reference to whisker position on a millisecond timescale.

Reducing spike count biases mice toward 'no' responses

Our photostimulation experiments show that mice did not use spike latencies with respect to a cycle-by-cycle representation of whisker position for object location discrimination. We next tested whether spike count in excitatory neurons could explain the behavioral choices of the mice. We optogenetically stimulated GABAergic neurons of the C2 column using VGAT-ChR2 mice (Fig. 7a; [39]), during the exploration window when mice whisked to sample the pole locations. Optogenetic inhibition reduced touch-evoked activity of excitatory neurons to 57% of baseline ($p=0.007$, paired two-tailed t-test; Methods). If mice rely on precise spike latency to decide between 'yes' and 'no' responses, then optogenetically reducing spike count should not differentially affect performance on YES and NO trials. However, if mice base their decision on spike count, then silencing should improve performance on NO trials but decrease performance on YES trials. Consistent with a spike count code, silencing on YES trials reduced performance (Fig. 7b; mean reduction in fraction trials correct, 0.43; all mice $p<0.001$, one-tailed permutation test), and silencing on NO trials improved performance (Fig. 7b; mean increase in fraction trials correct, 0.24; all mice $p<0.01$).

To rule out the possibility that mice simply were confused or otherwise stopped licking upon silencing, we performed the silencing experiment using the symmetric, lick-left/lick-right version of object location discrimination (cf. Fig. 5h). Under these conditions, performance on YES trials was also decreased (Fig. 7c; mean reduction in fraction trials correct, 0.37; all mice $p<0.001$), while performance on NO trials was increased (Fig. 7c; mean increase in fraction trials correct, 0.19; 3 mice $p<0.05$; 1 mouse $p=0.08$). Manipulating activity in the C2 column therefore shifts the balance between 'yes' and 'no' responses, such that more activity among excitatory neurons was associated with more 'yes' responses, and less activity with more 'no' responses. All together, our results suggest that mice measure spike count in an ensemble of L4 neurons to determine if touch occurred in the YES pole location (high spike count) or the NO pole location (low spike count) (Fig. 7d).

Illusory perception occurs only during tactile exploration

A preliminary trial-by-trial analysis suggested that illusory object perception was produced only if photostimulation coincided with task-related bouts of whisking (sFig. 8c). Because whisking often began shortly after the trial start cues (masking flash and the audible onset of pole movement) and continued through most of the exploration window, there were few trials in which photostimulation did not overlap whisking. To improve our statistical power we supplemented this dataset with two additional experiments. In these, we shifted the onset of the masking flash, which signaled trial start, earlier such that it preceded the pole motion by one second.

This prompted more variable onset of whisking in the exploration window, with clear separation between bouts of whisking and rest periods (whisking, $\theta_{amp} > 2.5$; Fig. 8a). To achieve photostimulation at variable times with respect to whisking bouts, we then photostimulated either (1) with 20 pulses at 20Hz (corresponding to the mean inter-photostimulus interval in the experiments of Fig. 5, 6; 0.053 ± 0.067 s, mean ± STD, n=68,552 intervals), initiated one second prior to pole motion, or (2) with pulses corresponding to the pattern of virtual pole crossings from five trials ago (as in 'shuffled light' trials; sFig. 8b, c), but shifted one second earlier within the trial than when they would normally occur (Methods). Trials of both types were then pooled with the earlier (sFig. 8b, c) 'shuffled light' trials. We sorted these pooled trials into 'Not whisking' and 'Whisking' categories based on whisking amplitude during photostimulation (Fig. 8b; sFig 8d–f). During whisking bouts, the mice expressed robust illusory YES responses (Fig. 8c). If photostimulation coincided with rest periods, the mice showed no signs of illusory YES perception ($p = 0.001$, 'Whisking' vs. 'Not whisking' trials pooled across mice, one-tailed permutation test). These experiments show that reports of perception of L4 activity are limited to bouts of tactile exploration when active touch normally occurs (sFig. 9a). In addition, L4 activity is ignored unless within the barrel corresponding to the moving whisker. Thus, perceptual reports of touch are gated by sensory expectation.

Discussion

Patterns of action potentials propagating through a hierarchy of neural circuits code for features of the world and our actions within it [14]. Making sense of such systems requires measurements of activity in defined circuit nodes to develop hypotheses about neural coding, and targeted perturbations to establish causal links between neural activity, perception and behavior [31,40,41].

Our experiments rely on cell type-specific [42], temporally precise, and quantitative photostimulation [38] to establish causal relationships between features of spike trains and perceptual behavior. Closed-loop control further allowed us to couple behavior and precise stimuli during active somatosensation. This real-time linkage between behavior and activity perturbations is important because normal perceptual behaviors are active [2,6,9,14,43]: representations of the environment are constructed from internal models of sensor movement and sensation [1]. Our study builds on pioneering work that used electrical microstimulation in simple perceptual tasks (e.g. motion direction discrimination, tactile

frequency discrimination) to link activity in defined brain regions to perception in passively stimulated animals [31,40].

Here we report that photostimulating a subset of L4 neurons was sufficient to evoke robust illusory touch sensation and perception of object location without training on photostimulation (Fig. 5). This is remarkable, because the overlap of L4 neurons phasically activated by touch and those activated by light is 50 % (Fig. 4e). Furthermore, photostimulation activated only a subset of somatosensory pathways, bypassing the paralemniscal pathway and the superior colliculus [44]. Differences between activity produced by photostimulation and touch might explain why photostimulation was rarely successful in fooling the mice completely (Fig. 5c, e).

During tactile behavior, L4 neuron spikes displayed exquisite latency precision which could be used to discriminate object locations (Fig. 3b, d). Despite this, several lines of evidence show mice determined pole position based on spike count rather than spike latency. First, adding spikes by L4 photostimulation on NO trials increased the proportion of 'yes' responses (Fig. 5c–e; sFig. 7). Second, decoupling L4 activity from whisker position in time did not change the degree of fooling (Fig. 6). Third, spike count decoded the behavioral choice better than spike latency (Fig. 3e). Fourth, on NO trials, touches were associated with a higher error rate ('yes' responses) compared to trials without touches (sFig. 7), indicating that mice did not use precise knowledge of whisker position at the time of contact in deciding on a response. Finally, reducing spike count systematically biased behavioral choice toward 'no' responses (Fig. 7).

Mice solved our task by preferentially moving their whiskers in the vicinity on one of two object locations, perhaps attempting to maximize the spike count difference between object locations [6,12]. This feature of the whisking strategy was similar for different pole positions (cf Fig. 1 and sFig. 5) and reward contingencies (cf Fig. 1 and sFig. 6). The whisking strategy is analogous to searching for one of two light switches in a dark room, a problem typically solved by biased probing, based on the remembered locations of the switches. One interpretation is that mice try to convert object location discrimination into a detection task (i.e. detecting the pole in one of the two locations). The spike count code used by the mice might be coupled to the behavioral strategy used by mice.

However, a spike count code could more generally tell the animal about object location. Freely moving rodents rapidly scan their whiskers through a range of interest, similar to the situation in our experiments. During natural behaviors the position of the range of interest in space is continually adjusted by head movements, and changes in the whisking setpoint [45]. Forces exerted by objects onto whiskers will differ with object location relative to the range of interest, providing spike count clues about object location, both in the azimuthal (sFig. 9) and radial directions [5,7].

Precise spike timing might still play roles in assessment of texture [46] or interactions between multiple whiskers [47]. Furthermore, certain aspects of spike timing are likely required in our task. Synchronous activity of L4 neurons, evoked by touch or photostimulation (Fig. 4c), may be essential for driving appropriate downstream ensembles.

Numerous reports have documented exquisite stimulus selectively in vS1 neurons, for instance for direction [23], velocity [48], and possibly even phase within the whisk cycle [27]. Future experiments, using similar methods as those introduced here, could reveal the conditions under which these different aspects of tactile information are actually read out to inform behavior.

Photostimulation of L4 neurons evoked illusory touch only during epochs of tactile exploration defined by whisking and the expectation of informative touch (Fig. 8). We do not know whether activity evoked outside these epochs of exploration was not perceived or simply not acted upon, for instance because the photostimulation-evoked sensation was unnatural or not interpretable due to the lack of appropriately coordinated sensory and motor activity patterns.

Multiple mechanisms likely collaborate in gating the stimulus-response chain between L4 activity and behavior. The vibrissal motor cortex (vM1) sends signals coding for whisking amplitude to L1 of vS1 [16]. Pyramidal cells in the barrel cortex receive this input in their tuft branches in L1, while bottom-up sensory input, in part from L4 neurons, impinges mainly on the proximal basal dendrites [25]. L1 input increases neuronal gain and can promote dendritic calcium spikes and bursting with coincident input in the proximal basal dendrites [30,49]. The whisker position signal from vM1 might selectively amplify activity related to touch during periods of tactile exploration. Similarly, cholinergic modulation and disinhibition might contribute in changing the gain of cortical networks during periods of attention [50].

Furthermore, illusory touch could only be evoked in a specific somatotopic location corresponding to the trained whisker (Fig. 5e, g). During learning, the brain presumably learns to selectively read out activity in this area and ignore activity in other regions of the barrel cortex and other sensory areas. The underlying mechanisms are unclear but might include top-down modulation, such as spatially selective attention and barrel cortex plasticity associated with learning. Similar experiments to those introduced here could be used to study fundamental mechanisms underlying spatial signal selection for optimal decision making.

Methods

All procedures were in accordance with protocols approved by the Janelia Farm Research Campus Institutional Animal Care and Use Committee. We report in vivo data from a total of 48 mice: L4 neuronal recordings, 9 mice (C57/Bl6) (Fig. 2,3); L4 photostimulation behavior experiments, 24 mice (10 Six3Cre [34] and 14 Scnn1a-Tg3-Cre [33]) (Fig. 4–6, 8); silencing, 6 VGAT-ChR2 mice[39] (Fig. 7); electrophysiological calibration of the light stimulus, 4 VGAT-ChR2 mice (Fig. 7); in vivo electrophysiology to calibrate photostimulation, 2 Six3Cre mice (2 Six3Cre and 6 Scnn1-Tg3-Cre mice were used for both behavior and calibration) (Fig. 4, sFig. 3); measurement of adaptation to photostimulation, 2 Ai32-x-Scnn1a-Tg3-Cre [51] mice (sFig. 4); behavioral light-detection experiment (sFig. 7f), 1 mouse (Tg(Etv1-cre)GM225Gsat with a sham infection). Additional mice were used for brain slice experiments (sFig. 10). Mice of the appropriate genotypes were assigned to experimental conditions arbitrarily without explicit randomization or experimenter blinding.

However, for roughly half the mice with virus injections, the experimenter was de facto blind to expression level until after all experiments were completed.

Object location discrimination task and high-speed videography

We used three variations on a whisker-based object location discrimination task described previously[6,12], with the following modifications: all mice performed the task using only the C2 whisker; use of a thinner stimulus pole (0.500 mm diameter class ZZ gage pin, Vermont Gage), which reduced passive contact of the whisker by the pole; no airpuff punishment; water was not pumped out of the lickport (i.e. the mouse did not compete with a peristaltic pump for water rewards), as we found that mice effectively consumed all water and pooling was not a problem. In the first variation (Figs. 1, 2, 3, 5ag, 6, 7b, 8), we used a go/no-go task, with the go stimulus location more posterior than the no-go stimulus (close to the resting position of the whisker) [6]. In silicon probe recording sessions, the go position was randomly chosen on each trial from a range of four relatively posterior positions spanning 4.29 mm [17]. In the second variation (Fig. 5h, 7c, sFig. 6), we used a lick-left/lick-right task in which both stimulus locations were rewarded. The posterior pole position required a lick at the right-side spout, whereas the anterior pole location required a lick at the left-side spout. If the mouse first licked at the incorrect spout, the trial was scored as incorrect and a timeout punishment was given. Trials without responses were rare (fewer than 2% of trials in the experiment of Fig. 5h). Typical bias toward one of the two lickports is shown in Fig. 7c. The third variation (sFig. 5) was a go/no-go task in which the rewarded (i.e. go) stimulus location was more anterior, further from the resting position of the whisker than the no-go stimulus. This change in the reward contingency produced markedly different whisking (sFig. 5b).

After mice achieved high performance with full whisker fields (typically > 80% correct), their right whiskers were trimmed to C-row whiskers (the left side was left untrimmed). After performance stabilized in this condition, mice were trimmed to C2.

We used an optical "lickport" to record licks and deliver water rewards for go/no-go experiments [6]. We also used a two-spout electrical lickport[52] for the lick-left/lick-right task and for some go/no-go sessions (with one spout disabled). The pole locations were 11.6–15.25 mm from midline and the anterior-posterior offset of the pole locations was 4.29–5.71 mm, corresponding to 23–30° of azimuthal angle.

Video (1 kHz) was acquired for at least 2 seconds per trial, starting before pole movement and ending after the response. Images were acquired with a Basler 504k camera and Streampix 3 software (Norpix), using a telecentric lens (Edmund Optics) and 940 nm illumination (Roithner Laser). Whisker tracking was performed with the Janelia Whisker Tracker (https://openwiki.janelia.org/wiki/display/MyersLab/Whisker+Tracking) [4,6]. Video frames with contact between whisker and pole were identified based on proximity between the whisker and pole and whisker curvature changes induced by the pole. In electrophysiology recordings all contacts were further inspected manually. We report here analysis of 147,269,000 frames of video from 70,756 behavioral trials during the ChR2 photostimulation experiment, plus an additional 13,896,000 frames of video from 3,088 behavioral trials from the L4 neuronal recording experiments.

Optogenetic targeting of cortical layer 4 neurons

We used two types of adult (>P60) male transgenic mice expressing Cre recombinase in L4 neurons (sFig. 10). In Scnn1a-Tg3-Cre mice[33](Jackson Labs: 009613, B6;C3-Tg(Scnn1a-cre)3Aibs/J), Cre expression is restricted to L4 stellate cells. Six3-Cre mice [25] were obtained by backcrossing Six3-Cre, line #69 for at least 9 generations to C57BL/6Crl mice (Charles River). These mice express Cre in both L4 stellate cells and L4 GABAergic neurons [33,34]. We used both types of mice in parallel because Scnn1a-Tg3-Cre mice also express Cre in the thalamus, whereas Six3-Cre mice do not. However, histological analysis of the experimental mice did not reveal retrograde infection and ChR2 expression in thalamic relay cells. Behavioral results using these two types of mice were indistinguishable (sFig. 10).

To restrict ChR2 expression to L4 neurons we used adeno-associated virus (serotype 2/5; AAV2/5- hSyn1-FLEX-hChR2-tdTomato). *hSyn1-FLEX-hChR2-tdTomato* was obtained by subcloning a PCR fragment containing the 930 bp human codon optimized channelrhodopsin-2 (hChR2), fused in frame to tdTomato [53] (linker: GCCGCGGCC), into an *AAV-hSyn1-FLEX* parent vector (gift of L. Looger) at Xba1 and Fse1 sites. The resulting plasmid (*pAAV-hSyn1-FLEX-hChR2-tdTomato*; Addgene 41015) contained the AAV inverted terminal repeats and a cassette with the human synapsin-1 promoter, a Cre-dependent [36] (double-floxed and inverted) open reading frame for hChR2-tdTomato, a woodchuck hepatitis post-transcriptional regulatory element (WPRE), and an SV40 polyA sequence. AAV2/5 virus was produced by the Janelia Farm Molecular Biology Shared Resource.

Mice were implanted with titanium headposts for head fixation [12]. Intrinsic signal imaging was performed through the skull [37] and a layer of cyanoacrylate adhesive (Krazy Glue), or Krazy Glue covered with clear nail polish (Electron Microscopy Sciences) to reduce glare. For anesthesia we used chlorprothixene (0.007 mg, IM, ~0.36 mg/kg; Sigma C1671) and isofluorane (~0.5 % in O_2).

After 1–13 days, we injected virus into the C2 or E3 barrels through a thinned region of skull under isoflurane anesthesia (1.5–2%). The injection system comprised a pulled glass pipette (~30 μm OD, either broken to a sharp edge or broken and then beveled; Drummond Scientific, Wiretrol II) back-filled with mineral oil. A fitted plunger was inserted into the pipette and slowly advanced to displace the contents using a hydraulic manipulator (Narashige, MO-10). We injected 10 nl at each of three depths: 600 μm, 500 μm, and 400 μm.

For a subset of the "sham infection" experiments (Fig. 5f; N=3 mice), we used AAV2/1-CAG-FLEX-hM4D-2A-GFP (gift from S. Sternson) containing the CAG promoter, a Cre-dependent *hM4D-2A-GFP* sequence [54], and WPRE and SV40 polyA sequences. For the remaining "sham infections," mice (N=2) were injected with AAV2/5- hSyn1-FLEX-hChR2-tdTomato, but in these experiments ChR2-tdTomato was not expressed for unknown reasons.

Virus expression was for 43–129 days (90 ± 25 days; mean ± STD) before the behavioral photostimulation session. The final behavioral photostimulation session occurred after 47–

183 days (105 ± 33; mean ± STD) of virus expression. After training, but prior to the first photostimulation session, we constructed a black dental acrylic (Lang Dental) 'well', leaving a ~2 mm diameter patch of skull over the C2 (or E3) column unobstructed.

After the experiments, mice were perfused transcardially with PBS followed by 4% PFA/0.1 M PB. To recover the location of ChR2 expression within the barrel map, the cortex was flattened between two glass slides, sectioned at 100 μm, and processed for cytochrome oxidase [12]. Images of ChR2-tdTomato fluorescence within the CO-stained barrel map were acquired on a macroscope (Olympus MVX10). The area showing ChR2-tdTomato labeled neurons was outlined manually (sFig. 2). For confocal imaging (Zeiss LSM 510) (Fig. 4a), coronal sections were mounted on glass slides using Vectashield mounting medium with DAPI [12].

Real-time control of cortical layer 4 neurons

Behavior and photostimulation were controlled by open-source software (http://brodylab.princeton.edu/bcontrol; Z. Mainen, C. Brody, C. Culianu) [6,12]. Analog outputs for controlling photostimuli and masking light flashes were from a PCI-6713 board (National Instruments). The virtual pole (diameter ~0.5 mm, determined by beam diameter and experimenter-chosen photodiode voltage thresholds) was a laser beam produced by a laser diode (Thorlabs, CPS808; wavelength, 808 nm). The position of the virtual pole was adjusted daily to lie next to one of the pole locations along the whisker. We imaged the intersection between the virtual pole and the whisker onto a photodiode (Hamamatsu, S9219). The light scattered by the whisker moving though the virtual pole was detected by the photodiode, amplified (Stanford Research Systems, Model SR570), and processed using the real-time control system (hard real-time task period, or worst-case timing jitter, 0.1667 ms). Two intensity thresholds were set for each session. As the whisker passed through the virtual pole, first the low and then the high threshold was exceeded. When the photodiode signal exceeded the higher threshold the whisker was considered to have 'crossed' the virtual pole. A new crossing could not occur until the photodiode signal dropped below the lower threshold.

Light from a 473 nm laser (CL-473-150, Crystal Laser) was gated by an acousto-optical modulator (AOM; MTS110-A3-VIS, Quanta Tech; extinction ratio 1:2000) and a shutter (Vincent Associates) under control of the real-time Linux system. Light exiting the AOM was focused into a multimode optical fiber (62.5 μm; Thorlabs) and recollimated. Each day the beam was positioned over the C2 or E3 column. The beam diameter was ~1.5 mm (99% of energy).

Laser pulses were delivered to the brain through the skull, which was occasionally thinned; a thin layer of Krazy Glue; a thin layer of non-pigmented dental acrylic (Lang Dental). Laser power at the surface of this preparation was set for a given session at either ~73 mW (pulse duration of 1 ms), or at ~56 mW (pulse duration of 1.333 ms) (intensities ~32–41 mW/mm^2). For 6/34 "sham" (ChR2-negative) sessions, we increased the dose to ~57 mW and 2 ms.

A separate data acquisition computer running *Ephus* (ephus.org) acquired the photodiode signal, the AOM control signal, and triggered individual frames of high-speed video (all on the same clock, triggered by a master trigger from the real-time Linux system). This allowed us to align high-speed video frames with virtual pole crossings and photostimulation pulses, without compensation for computer clock drifts.

To minimize the possibility that mice would see and respond to light pulses per se (i.e. independent of neuronal excitation), on every trial a 'masking flash' pulse train (20 pulses at 10 Hz, 1–2 ms per pulse) was delivered using a custom LED driver and 470 nm LEDs (Luxeon Star), positioned near the eyes of the mouse. The masking flash began as the pole started moving into reach and continued through the end of the period in which optogenetic pulses could occur. For experiments in which optogenetic pulses occurred prior to the start of pole movement ('early' light pulses; Fig. 8), the masking flash began one second prior to pole motion and 30 masking flash pulses were delivered instead of 20. Mice were unable to solve the object location discrimination task visually. Performance of highly trained mice dropped to chance levels after the C2 whisker was trimmed (lick-left/lick-right; $n = 2$, lick/no lick; $n = 3$; $p > 0.26$).

Optogenetic silencing of barrel cortex

VGAT-ChR2 mice were surgically implanted with custom stainless steel or titanium headposts for head fixation and the dorsal surface of the skull was covered in Krazy Glue followed by a layer of clear dental acrylic (Lang Dental) which was polished using acrypoints (Acrylic Polishing Kit HP Shank, Pearson Dental). A thin layer of clear nail polish (Electron Microscopy Sciences, 72180) was applied to reduce light glare. Silencing was with 473 nm laser light centered on C2 through the polished skull, producing silencing in a tissue volume with radius 1 mm and comprising all layers (ZVG, NL, KS, et al submitted).

For the lick/no-lick experiment (Fig. 7b), the photostimulus was a pulse train (5 ms square wave pulses; 50 Hz; average power, 4 mW, CL-473-150, Crystal Laser) delivered with masking flash (1–2ms at 10Hz) beginning at the onset of pole motion for a fixed duration of 3.75 s. Silencing trials were a randomly chosen 25% of all trials. Data are means of trials pooled over 1–4 sessions per mouse and show 24–44 silencing trials per session and 44–151 silencing trials total per mouse (Fig. 7b).

For the symmetric response, lick-left/lick-right experiment (Fig. 7c), stimulation was at ~2 mW mean power delivered either continuously or using a train of 1 ms square wave at 80 Hz. The photostimulus began at the onset of pole movement for a fixed duration of 1.5 s (ending after the response cue, described below). Silencing trials were a randomly chosen 25% of all trials, never back to back. In addition, the symmetric response silencing experiment differed from the earlier experiments reported here in the following details: At the beginning of the exploration window, the vertical pole moved quickly (0.2 s) into reach of the C2 whisker, whereupon the mouse whisked to make contact with the pole. The pole was present for 1 second; the exploration window terminated when the vertical pole moved (0.2 s) out of reach of the C2 whisker. During the exploration window, mice were trained to withhold their licking response. After the exploration window, an auditory "response" cue

(pure tone, 3.4 kHz, 0.1 s duration, DigiKey, 458-1088-ND) was issued and mice initiated licking. Licking early during the trial was punished by a loud "alarm" sound (siren buzzer, 0.05 s duration, RadioShack, 273–079), followed by a brief timeout (1–1.2 s). Continued licking triggered additional timeouts. The trial was allowed to resume once the timeout was complete, but these trials were excluded from the analyses. Data (Fig. 7c) are means of trials pooled over 3–6 (4.3 ± 1.2, mean ± SD) sessions and comprised 66 ± 17 (mean ± SD) silencing trials per photostimulation condition (continuous or pulse) per mouse.

In vivo electrophysiology

Spikes during the object location discrimination task were recorded either using loose-seal cell-attached recordings [12] or silicon probe recordings. After a loose seal was achieved, the behavioral protocol was initiated for 5–15 trials. Cells which did not exhibit task-modulated activity were discarded. Numbers reporting fraction of touch modulated neurons were derived from previous loose seal recordings [12].

For silicon probe recordings, on the first day of recording a 1mm diameter craniotomy was opened above the C2 column. The dura was retracted using fine forceps (Dumot #5SF). We used probes with 32 pads distributed across four shanks (Neuronexus Buzsaki32-A32 and Buzsaki32Lsp-A32). Prior to each recording, the tips of the probe were brushed with DiI. The animal was briefly anesthetized (2–3 minutes @ 1.5% isoflurane) to remove the cement and silicon cap. The mouse was then mounted in the behavioral and recording apparatus. The probe was positioned on the surface of the cortex and photographed. Two drops of 1.5% Type III-A agarose in cortex buffer were applied to the well. The probe was lowered (1–2 μm/s pausing 60 s every 30–50 μm) into the brain normal to the pial surface. If any of the shanks began to bend, or the cortex dimpled, the probe and agarose were removed, and the process restarted. Animals were awake and clam during probe descent. Behavioral protocols were initiated after probe location was finalized. Each behavioral session time, including probe insertion and removal lasted 1.5–2.5 hours. Following a recording session the well was filled with Kwik-Cast (WPI) and sealed with dental cement. On subsequent days (2–6 total days per animal), the electrode was positioned > 100 μm from previous recording sites.

After the experiment brains were fixed and the brain blocked at ~30° from the horizontal. The brain was lightly compressed between two glass slides, which flattened the barrel field. Slices were cut tangential to the cortical surface (100 μm thickness) and stained for cytochrome oxidase. DiI spots and the surface photography were used to map recording day to location in the barrel map. Recording location was defined by triangulating the position of the center of each DiI spot to the three nearest barrels, then warping these points to a standard barrel map [55]. Putative layer 4 recordings were limited to sessions where the manipulator depth from surface minus distance from tip to pad with maximum spike energy was 418–588 μm and the DiI spot terminated in either the slice containing the CO staining or the next deeper slice.

Si probe voltage traces were digitized at 19531.25Hz and stored using a custom headstage (Brian Barbarits, Tim Harris, www.janelia.org/lab/apig-harris-lab) and custom software (Calin Culianu, Anthony Leonardo). Raw voltage traces were bandpass filtered between 300 and 6,000 Hz (MATLAB 'idealfilter'). Common source noise was removed by sorting all 32

traces by amplitude for each timepoint, then subtracting the mean voltage of the middle 50% of sorted traces from each unsorted trace. Spikes were detected independently for each channel as threshold crossings above 4 STD of the channel. Events whose peak amplitudes across channels on the same shank occurred with <307.5μs jitter were merged. For each event, waveforms for all eight channels on the shank were extracted and upsampled 2x. PCA was performed on individual channels for all waveforms in the recording session that exceeded 4 STD.

Putative single units were sorted by manual cutting in MatClust [56]. Each shank was sorted separately. Sorting parameters were spike amplitude, width and first two principal components for all eight channels plus time (33 total parameters). Following sorting, quality metrics were calculated [57]. Estimated false negatives from undetected spikes below voltage threshold were <0.1% for all units. Estimated false negatives from censored period exclusion ranged 1.6–4.7%, mean 3.6 ± 1.0%. Estimated false positives from ISI violations between the censored and absolute refractory period ranged 0–12.8% mean 1.2 ± 3.0%, assuming a 10Hz, independent, Poisson-spiking contaminating unit. A total of 148 units were sorted (mean 7 per recording) of which 21 met distance (<250 μm from C2 center) and depth (see above) criteria to be considered near-C2, L4 units.

Comparison of the cell-attached to silicon probe dataset showed no significant difference in touch latency (mean, 8.6 cell-attached vs. 9.0 ms silicon probe), jitter (mean 4.8 vs. 5.9 ms), decoding of behavioral choice (mean AUC, spike count, 0.675 vs. 0.650; spike-triggered theta, 0.610 vs. 0.587), spike count decoding of pole location (0.626 vs. 0.593), and evoked spikes per first contact (mean 1.00 vs. 1.55). Cell-attached units had nearly significant lower baseline firing rates (mean 5.1 vs. 13.2 Hz, $p = 0.11$), and significantly better spike-triggered decoding of pole position (0.658 vs. 0.602; $p = 0.012$). These data suggest silicon probe recordings may have a sampling bias for a functionally similar but more active set of L4 neurons than cell-attached recordings.

To calibrate the photostimulation pulses, we performed loose cell-attached recordings in awake mice in the behavior apparatus [12], with the following modifications: (1) we covered the recording well and craniotomy with HEPES-buffered artificial cerebrospinal fluid rather than a thick layer of agarose; and (2) the craniotomy was larger (up to 1.5 mm in diameter). Eight of ten mice were the same mice used for behavior experiments; the remaining two mice were prepared identically. Pulses occurred every 20 s. For each neuron we stepped sequentially through pulses comprising 100%, 66%, 40% and (in most cases) 20% of maximum power, with a mean of 29 sweeps per neuron. The latency and number of evoked spikes were relatively weak functions of the applied light intensity in L4 (Fig. 4b; sFig 3). Maximum power was matched to our behavioral experiments (53 ± 3.6 mW, mean ± STD; range 45–57 mW; N=85 neurons). Pulse duration was adjusted to roughly standardize the maximal light dose (1.38 ± 0.09 ms; range 1.333 – 1.667 ms). Because of the trade-off between maximum intensity and pulse duration, to pool neurons we occasionally report "Relative power" as a percentage of the maximum power (sFig. 3e, f).

To determine the reliability of L4 photostimulation-evoked responses during trains matching the whisking pattern, we recorded from ChR2+ cells in loose-seal mode while replaying

photostimulation trains corresponding to whisking patterns in other experiments. For these recordings (sFig. 4) we used mice derived from a cross between Scnn1a-Tg3-Cre and AI32 (a channelrhodopsin-2 Cre reporter; [51]). For each cell, twenty different trains of 1ms pulses were delivered at a light intensity of 2–3x the minimal power required to evoke a spike (range 0.85–2.5 mW, sFig. 4). Spike latencies for each cell showed very low variability (mean STD = 0.59 ms) and were only weakly dependent on interstimulus interval (sFig. 4b). The probability of a spike being evoked by photostimulation was dependent on the interstimulus interval, with short intervals correlated to a reduced spike probability (sFig. 4c). However, short interstimulus intervals were relatively rare and the spike probability was on average a flat function of the sequential photostimulus number (i.e., first, second, etc.; sFig. 4d).

To characterize inhibition by photostimulation of GABAergic neurons in VGAT-ChR2 mice (Fig. 7a) we made Si probe recordings near the C2 barrel column while mice performed the lick-left/lick-right task. Single units were sorted manually offline. We characterized cells with broad action potentials that were not excited by photostimulation. These are putative excitatory neurons. We further selected neurons that were rapidly excited by touch (5–25 ms time window) with 10–20 photostimulus trials (25% of all trials).

Data analysis

The 'exploration window' comprised the period from the start cues, the start of pole movement and/or masking flash, until the answer lick response or until 1.5 s later (capturing ~99% of reaction times), whichever came earlier. For presentation in figures, traces of the whisker base angle, θ, were smoothed with a 5-ms moving average.

For decoding analyses (Fig. 3), we computed the area under the receiver-operating characteristic (ROC) curve (MATLAB 'perfcurve'), using as the decision variable either: (1) the total spike count within the exploration window, n_s; or (2) mean spike-triggered theta, θ_s. Each neuron was considered independently. We assumed for decoding that the correct 'sign' (i.e. the class giving higher decision variable values) was known. That is, in predicting the class (object location or yes/no choice) for a given trial based on the value of the decision variable, we treated higher decision variable values as predicting the class that had the higher mean decision variable value. Thus, values of AUC less than chance level (AUC = 0.5) could only occur for non-discriminative neurons. We included trials both with and without contact.

For the analysis of Fooling Index (FI) versus whisker angle at stimulation (Fig. 6c), we computed FI_i as

$$\mathrm{FI}_i = \mathrm{yes}_{\mathrm{stim},i} - \mathrm{yes}_{\mathrm{ns}}.$$

$\mathrm{yes}_{\mathrm{stim},i}$ is the fraction of 'yes' responses on trials where θ five ms before the time of the first light pulse was in the *i*-th bin, and $\mathrm{yes}_{\mathrm{ns}}$ is the overall fraction of 'yes' responses on unstimulated NO trials within the session.

Whisking amplitude (θ_{amp}) was defined as the magnitude of the Hilbert transform of bandpass (6 to 60 Hz, Butterworth) filtered θ [17]. For the 'shuffled' light experiments (sFig. 8b,c), we chose a delay of five trials ('*N-5*'). Five trials was sufficiently short to ensure that the behavioral state (satiety, kinematics of whisking, etc) of the mouse was constant, and sufficiently long to avoid occasional response dependencies over 1–2 trials (e.g. impulsive licking). For the analysis of whisking-dependence of illusory object perception (Fig. 8), we considered light stimuli to occur during 'whisking' when the mean θ_{amp} at the time of the light pulses was greater than 2.5 degrees, only counting light pulses occurring prior to the end of the exploration window. We pooled trials from the 'shuffled' experiments described in sFig. 8b, c, as well as from new experiments in which light pulses were moved 1 s earlier in time ('early' light pulses). These 'early' light sessions were either (1) 'shuffled' light sessions in that the light pulses on trial *N* were taken from crossings on trial *N*-5, and then moved 1 s earlier, or (2) 'regular' light sessions in which a train of 20 pulses at 20 Hz (1–1.333 ms pulse duration) was delivered 1 s prior to the start of the pole movement (i.e. 1 s prior to the earliest time pulses could arrive during the basic experiment shown in Fig. 5).

Error bar SEM values were calculated using bootstrap methods. We did not predetermine sample size using power analysis.

Supplementary Material

Refer to Web version on PubMed Central for supplementary material.

Acknowledgments

We thank Matt Smear, Mac Hooks, Leopoldo Petreanu, Nick Sofroniew, Albert Lee, Hongdian Yang, David Golomb and Josh Dudman for comments on the manuscript, Nick Sofroniew for valuable suggestions on experiments, Susan Michael for histology, Tim Harris, Brian Barbarits, Anthony Leonardo, Vijay Iyer, Diego Gutnisky for help with silicon probe recordings, Mathias Karlsson for help with spike clustering.

References

1. Wolpert DM, Flanagan JR. Motor prediction. Current biology: CB. 2001; 11:R729–732. [PubMed: 11566114]
2. Knutsen PM, Pietr M, Ahissar E. Haptic object localization in the vibrissal system: behavior and performance. J Neurosci. 2006; 26:8451–8464. [PubMed: 16914670]
3. Voigts J, Sakmann B, Celikel T. Unsupervised whisker tracking in unrestrained behaving animals. J Neurophysiol. 2008; 100:504–515. [PubMed: 18463190]
4. Clack NG, et al. Automated tracking of whiskers in videos of head fixed rodents. PLoS computational biology. 2012; 8:e1002591.10.1371/journal.pcbi.1002591 [PubMed: 22792058]
5. Pammer L, et al. The Mechanical Variables Underlying Object Localization along the Axis of the Whisker. The Journal of neuroscience: the official journal of the Society for Neuroscience. 2013; 33:6726–6741.10.1523/JNEUROSCI.4316-12.2013 [PubMed: 23595731]
6. O'Connor DH, et al. Vibrissa-based object localization in head-fixed mice. J Neurosci. 2010; 30:1947–1967. [PubMed: 20130203]
7. Bagdasarian K, et al. Pre-neuronal morphological processing of object location by individual whiskers. Nature neuroscience. 2013; 16:622–631.10.1038/nn.3378 [PubMed: 23563582]
8. Kleinfeld D, Deschenes M. Neuronal basis for object location in the vibrissa scanning sensorimotor system. Neuron. 2011; 72:455–468.10.1016/j.neuron.2011.10.009 [PubMed: 22078505]
9. Mehta SB, Whitmer D, Figueroa R, Williams BA, Kleinfeld D. Active spatial perception in the vibrissa scanning sensorimotor system. PLoS Biol. 2007; 5:e15. [PubMed: 17227143]

10. Knutsen PM, Ahissar E. Orthogonal coding of object location. Trends in neurosciences. 2009; 32:101–109.10.1016/j.tins.2008.10.002 [PubMed: 19070909]
11. Hutson KA, Masterton RB. The sensory contribution of a single vibrissa's cortical barrel. J Neurophysiol. 1986; 56:1196–1223. [PubMed: 3783236]
12. O'Connor DH, Peron SP, Huber D, Svoboda K. Neural activity in barrel cortex underlying vibrissa-based object localization in mice. Neuron. 2010; 67:1048–1061. [PubMed: 20869600]
13. de Kock CP, Bruno RM, Spors H, Sakmann B. Layer- and cell-type-specific suprathreshold stimulus representation in rat primary somatosensory cortex. J Physiol. 2007; 581:139–154. [PubMed: 17317752]
14. Diamond ME, von Heimendahl M, Knutsen PM, Kleinfeld D, Ahissar E. 'Where' and 'what' in the whisker sensorimotor system. Nat Rev Neurosci. 2008; 9:601–612. [PubMed: 18641667]
15. Hill DN, Curtis JC, Moore JD, Kleinfeld D. Primary motor cortex reports efferent control of vibrissa motion on multiple timescales. Neuron. 2011; 72:344–356.10.1016/j.neuron.2011.09.020 [PubMed: 22017992]
16. Petreanu L, et al. Activity in motor-sensory projections reveals distributed coding in somatosensation. Nature. 2012; 489:299–303.10.1038/nature11321 [PubMed: 22922646]
17. Huber D, et al. Multiple dynamic representations in the motor cortex during sensorimotor learning. Nature. 2012; 484:473–478.10.1038/nature11039 [PubMed: 22538608]
18. Poulet JF, Fernandez LM, Crochet S, Petersen CC. Thalamic control of cortical states. Nature neuroscience. 2012; 15:370–372.10.1038/nn.3035 [PubMed: 22267163]
19. Yu C, Derdikman D, Haidarliu S, Ahissar E. Parallel thalamic pathways for whisking and touch signals in the rat. PLoS biology. 2006; 4:e124.10.1371/journal.pbio.0040124 [PubMed: 16605304]
20. Fee MS, Mitra PP, Kleinfeld D. Central versus peripheral determinants of patterned spike activity in rat vibrissa cortex during whisking. J Neurophysiol. 1997; 78:1144–1149. [PubMed: 9307141]
21. Crochet S, Petersen CC. Correlating whisker behavior with membrane potential in barrel cortex of awake mice. Nat Neurosci. 2006; 9:608–610. [PubMed: 16617340]
22. Lefort S, Tomm C, Floyd Sarria JC, Petersen CC. The excitatory neuronal network of the C2 barrel column in mouse primary somatosensory cortex. Neuron. 2009; 61:301–316. [PubMed: 19186171]
23. Simons DJ. Temporal and spatial integration in the rat SI vibrissa cortex. Journal of neurophysiology. 1985; 54:615–635. [PubMed: 4045540]
24. Armstrong-James M, Fox K, Das-Gupta A. Flow of excitation within rat barrel cortex on striking a single vibrissa. J Neurosci. 1992; 68:1345–1354.
25. Petreanu L, Mao T, Sternson SM, Svoboda K. The subcellular organization of neocortical excitatory connections. Nature. 2009; 457:1142–1145. [PubMed: 19151697]
26. Lu SM, Lin RCS. Thalamic afferents of the rat barrel cortex: a light- and electron-microscopic study using *Phaseolus vulgaris* leucoagglutinin as an anterograde tracer. Somatosens Mot Res. 1993; 10:1–16. [PubMed: 8484292]
27. Curtis JC, Kleinfeld D. Phase-to-rate transformations encode touch in cortical neurons of a scanning sensorimotor system. Nat Neurosci. 2009; 12:492–501. [PubMed: 19270688]
28. Boyden ES, Zhang F, Bamberg E, Nagel G, Deisseroth K. Millisecond-timescale, genetically targeted optical control of neural activity. Nat Neurosci. 2005; 8:1263–1268. [PubMed: 16116447]
29. Li X, et al. Fast noninvasive activation and inhibition of neural and network activity by vertebrate rhodopsin and green algae channelrhodopsin. Proc Natl Acad Sci U S A. 2005; 102:17816–17821. [PubMed: 16306259]
30. Xu NL, et al. Nonlinear dendritic integration of sensory and motor input during an active sensing task. Nature. 2012; 492:247–251.10.1038/nature11601 [PubMed: 23143335]
31. Romo R, Hernandez A, Zainos A, Brody CD, Lemus L. Sensing without touching: psychophysical performance based on cortical microstimulation. Neuron. 2000; 26:273–278. [PubMed: 10798410]
32. Histed MH, Ni AM, Maunsell JH. Insights into cortical mechanisms of behavior from microstimulation experiments. Prog Neurobiol. 201210.1016/j.pneurobio.2012.01.006
33. Madisen L, et al. A robust and high-throughput Cre reporting and characterization system for the whole mouse brain. Nat Neurosci. 2010; 13:133–140. [PubMed: 20023653]

34. Liao GY, Xu B. Cre Recombinase-mediated Gene Deletion in Layer 4 of Murine Sensory Cortical Areas. Genesis. 2008; 46:289–293. [PubMed: 18543315]
35. Nagel G, et al. Channelrhodopsin-2, a directly light-gated cation-selective membrane channel. Proc Natl Acad Sci U S A. 2003; 100:13940–13945. [PubMed: 14615590]
36. Atasoy D, Aponte Y, Su HH, Sternson SM. A FLEX switch targets Channelrhodopsin-2 to multiple cell types for imaging and long-range circuit mapping. J Neurosci. 2008; 28:7025–7030. [PubMed: 18614669]
37. Masino SA, Kwon MC, Dory Y, Frostig RD. Characterization of functional organization within rat barrel cortex using intrinsic signal optical imaging through a thinned skull. Proceedings of the National Academy of Sciences of the United States of America. 1993; 90:9998–10002. [PubMed: 8234348]
38. Huber D, et al. Sparse optical microstimulation in barrel cortex drives learned behaviour in freely moving mice. Nature. 2008; 451:61–64. [PubMed: 18094685]
39. Zhao S, et al. Cell type-specific channelrhodopsin-2 transgenic mice for optogenetic dissection of neural circuitry function. Nature methods. 2011; 8:745–752. [PubMed: 21985008]
40. Salzman CD, Britten KH, Newsome WT. Cortical microstimulation influences perceptual judgements of motion direction. Nature. 1990; 346:174–177. [PubMed: 2366872]
41. O'Connor DH, Huber D, Svoboda K. Reverse engineering the mouse brain. Nature. 2009; 461:923–929. [PubMed: 19829372]
42. Luo L, Callaway EM, Svoboda K. Genetic dissection of neural circuits. Neuron. 2008; 57:634–660. [PubMed: 18341986]
43. Yarbus, AL. Eye Movements and Vision. Plenum Press; 1967.
44. Veinante P, Lavallee P, Deschenes M. Corticothalamic projections from layer 5 of the vibrissal barrel cortex in the rat. J Comp Neurol. 2000; 424:197–204. [PubMed: 10906697]
45. Mitchinson B, et al. Active vibrissal sensing in rodents and marsupials. Philosophical transactions of the Royal Society of London Series B, Biological sciences. 2011; 366:3037–3048.10.1098/rstb.2011.0156 [PubMed: 21969685]
46. Jadhav SP, Wolfe J, Feldman DE. Sparse temporal coding of elementary tactile features during active whisker sensation. Nat Neurosci. 2009; 12:792–800. [PubMed: 19430473]
47. Panzeri S, Petersen RS, Schultz SR, Lebedev M, Diamond ME. The role of spike timing in the coding of stimulus location in rat somatosensory cortex. Neuron. 2001; 29:769–777. [PubMed: 11301035]
48. Pinto DJ, Brumberg JC, Simons DJ. Circuit dynamics and coding strategies in rodent somatosensory cortex. J Neurophysiol. 2000; 83:1158–1166. [PubMed: 10712446]
49. Larkum ME, Senn W, Luscher HR. Top-down dendritic input increases the gain of layer 5 pyramidal neurons. Cereb Cortex. 2004; 14:1059–1070. [PubMed: 15115747]
50. Letzkus JJ, et al. A disinhibitory microcircuit for associative fear learning in the auditory cortex. Nature. 2011; 480:331–335.10.1038/nature10674 [PubMed: 22158104]
51. Madisen L, et al. A toolbox of Cre-dependent optogenetic transgenic mice for light-induced activation and silencing. Nature neuroscience. 2012; 15:793–802.10.1038/nn.3078 [PubMed: 22446880]
52. Slotnick B. A simple 2-transistor touch or lick detector circuit. J Exp Anal Behav. 2009; 91:253–255.10.1901/jeab.2009.91-253 [PubMed: 19794837]
53. Shaner NC, et al. Improved monomeric red, orange and yellow fluorescent proteins derived from Discosoma sp. red fluorescent protein. Nat Biotechnol. 2004
54. Armbruster BN, Li X, Pausch MH, Herlitze S, Roth BL. Evolving the lock to fit the key to create a family of G protein-coupled receptors potently activated by an inert ligand. Proc Natl Acad Sci U S A. 2007; 104:5163–5168. [PubMed: 17360345]
55. Maier DL, et al. Disrupted cortical map and absence of cortical barrels in growth-associated protein (GAP)-43 knockout mice. Proceedings of the National Academy of Sciences of the United States of America. 1999; 96:9397–9402. [PubMed: 10430954]
56. Karlsson MP, Frank LM. Network dynamics underlying the formation of sparse, informative representations in the hippocampus. The Journal of neuroscience: the official journal of the

Society for Neuroscience. 2008; 28:14271–14281.10.1523/JNEUROSCI.4261-08.2008 [PubMed: 19109508]

57. Hill DN, Mehta SB, Kleinfeld D. Quality metrics to accompany spike sorting of extracellular signals. The Journal of neuroscience: the official journal of the Society for Neuroscience. 2011; 31:8699–8705.10.1523/JNEUROSCI.0971-11.2011. [PubMed: 21677152]

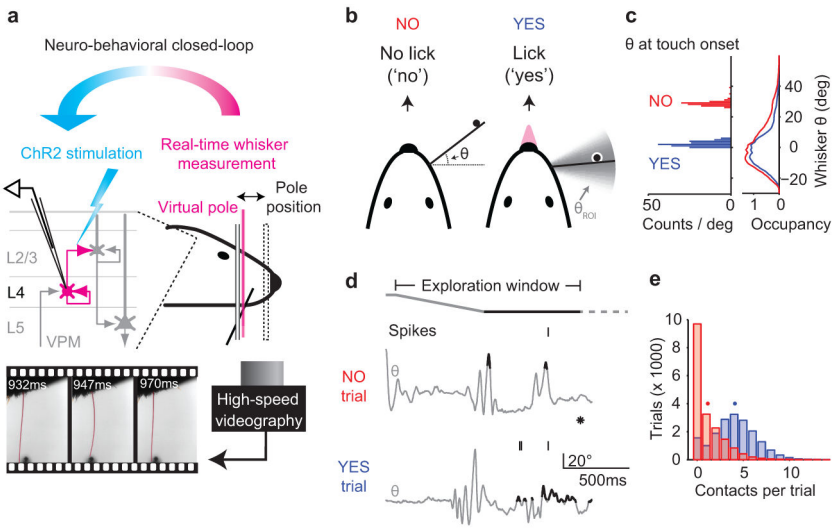

Figure 1. Overview of the experimental system and whisking strategy during object location discrimination

a. Recordings were made from L4 neurons while mice localized objects with the C2 whisker. Whisker movements were measured with high-speed video. The mouse indicated its decision by licking for a water reward. Whiskers were detected as they crossed a virtual pole (an infrared laser). A real-time system controlled photostimulation of ChR2-positive L4 neurons based on whisker position.

b. Schematic of the object location discrimination task. θ is the azimuthal angle of the whisker at the base.

c. Whisking during object location discrimination (data from one representative session). Left, whisker θ at touch onset (408 touches; YES trials, blue; NO trials, red). Right, distribution of whisker positions during task-related whisking (θ_{amp} > 2.5 degrees). Occupancy (in seconds) is the time spent at particular θ (bin size, one degree).

d. Whisker movements (grey; θ) in two example behavioral trials (top, NO trial; bottom, YES trial). Black trace segments correspond to contact periods. Pole entry (grey) and availability (black) indicated by uppermost line. Protraction corresponds to increasing θ. Ticks, spikes; asterisk, lick.

e. The number of contacts per trial for all sessions (36,910 trials; YES trials, blue; NO trials, red). Dots, means.

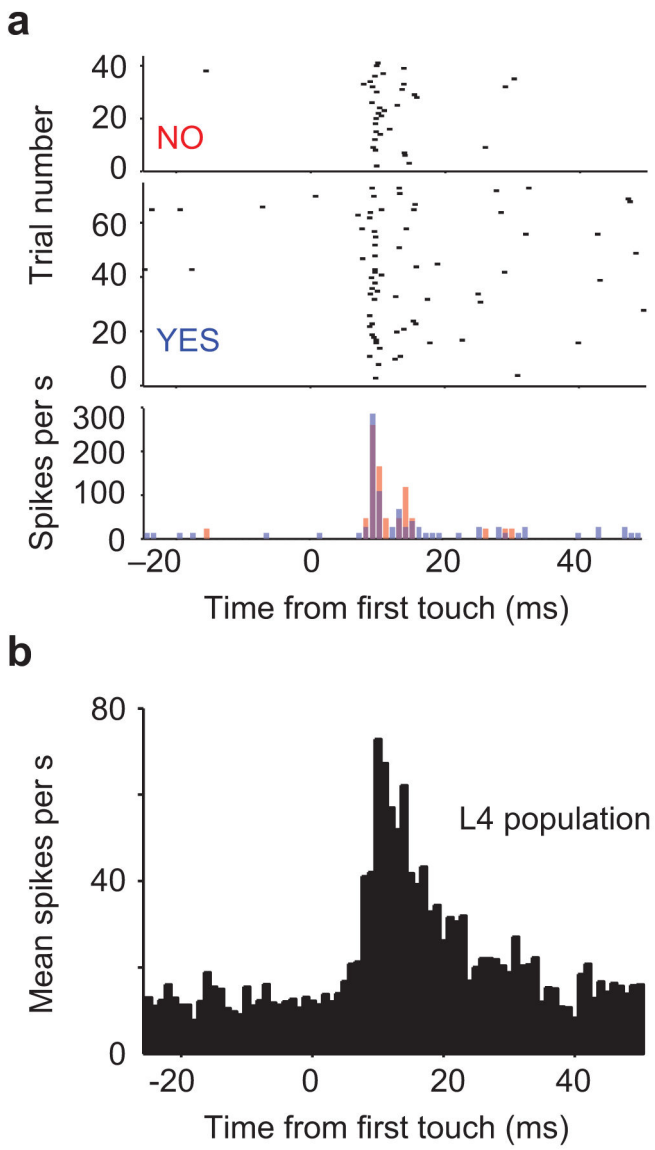

Figure 2. L4 neurons spike with precise latencies during object location discrimination

a. Spike rasters and peri-touch spike histogram for one L4 neuron aligned to first touch (same session as in Fig. 1d).

b. Peri-touch spike histogram averaged across all rapidly touch excited L4 neurons < 250μm from C2 center (13 neurons) for the first touch per trial.

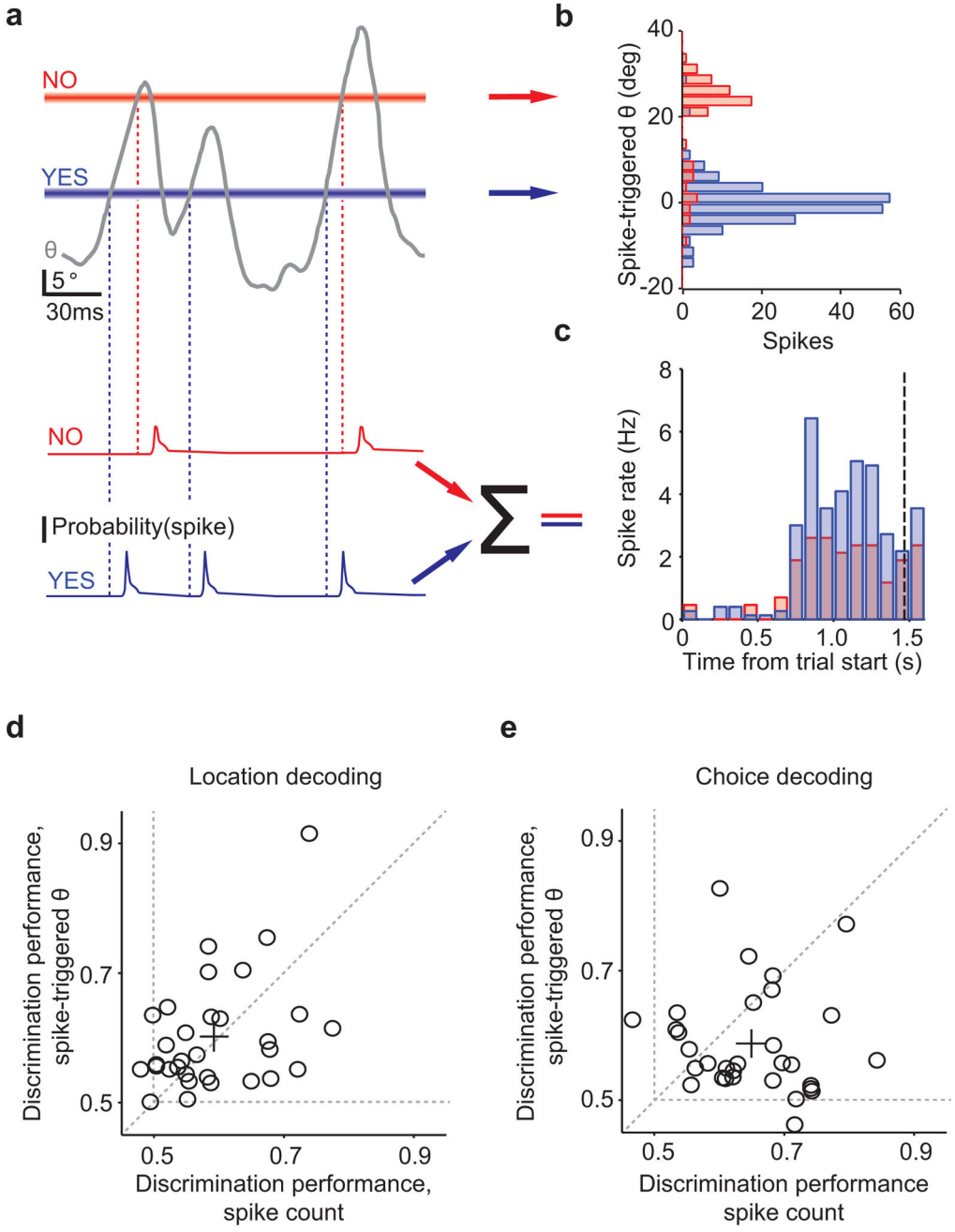

Figure 3. Decoding object location and behavioral choice based on L4 spikes

a. Neural coding of object location. Top, whisker position (θ, grey) and the two pole locations (blue, YES; red, NO). Bottom, schematic spike probability for the two object locations.

b. Spike-triggered θ (for every spike in the exploration window, adjusted by spike latency 9 ms) (YES trials, blue, n = 73; NO trials, red, n = 42; same as in Fig. 2a).

c. Spike count during the exploration window (same data as in Fig. 2a). Dotted line, mean reaction time.

d. L4 neurons discriminate object location equally based on spike count and spike-triggered θ (black circles, individual neurons; black cross, population mean and standard error; p = 0.57 paired two tailed t-test). 'Discrimination performance' is the area under the receiver operating characteristic curve for a linear classifier. Dotted lines, chance discrimination performance and equal discrimination performance.

e. L4 neurons discriminate behavioral choice based on spike count better than spike-triggered θ (p = 0.0085).

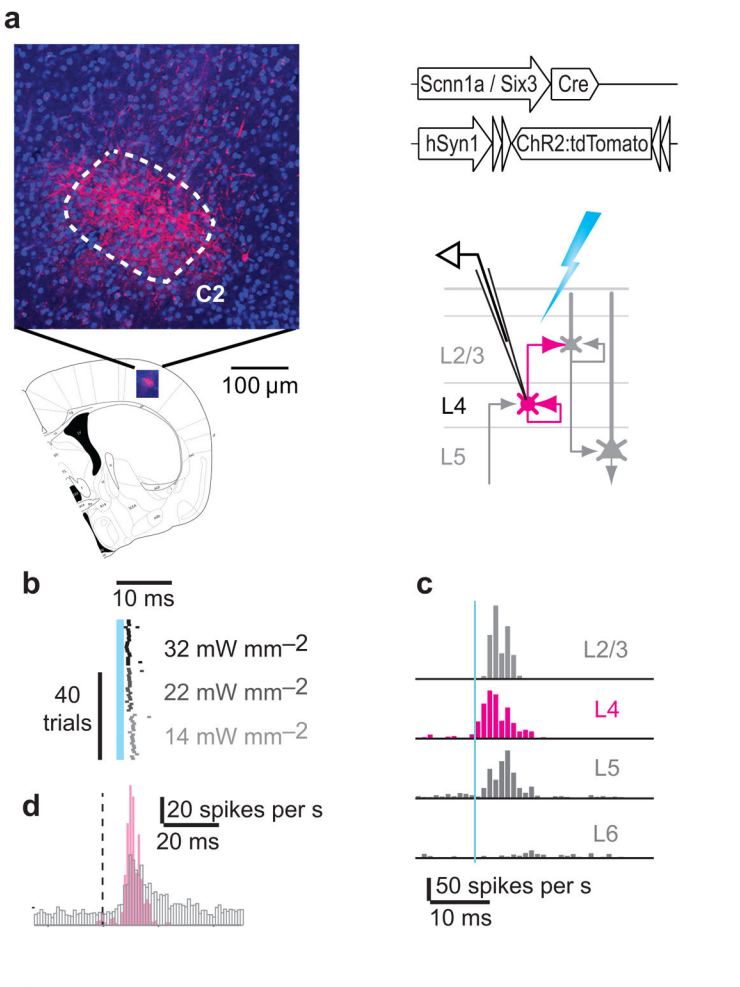

e

	Touch	Light
Neurons modulated by stimulus (%)	78	50
Spikes per stimulus	1.77 ± 0.77	1.03 ± 1.22
Latencies across cells (mean ± std, ms)	8.69 ± 3.01	2.3 ± 1.2
Latency jitter across cells (mean ± std, ms)	5.16 ± 1.32	0.58 ± 0.39
Duration of population activity (FWHM, ms)	7.72	4.73

Figure 4. Optogenetic stimulation of L4 neurons mimics touch-evoked spiking

a. Targeting ChR2 to L4 neurons. Left, ChR2-expression (magenta) in one barrel. Right, genetic scheme.

b. Single example neuron responding to different light intensities. Cyan, photostimulus.

c. Population peri-stimulus time histograms recorded in different cortical layers (n=85 neurons total), following a ChR2 stimulus. Responses are averaged across light intensities (Methods).

d. Overlay of population peri-stimulus time histogram (grey, touch; same data as Fig. 2b; magenta, photostimulation, delayed by 5 ms from stim).

e. Comparison of L4 activity evoked by touch and photostimulation.

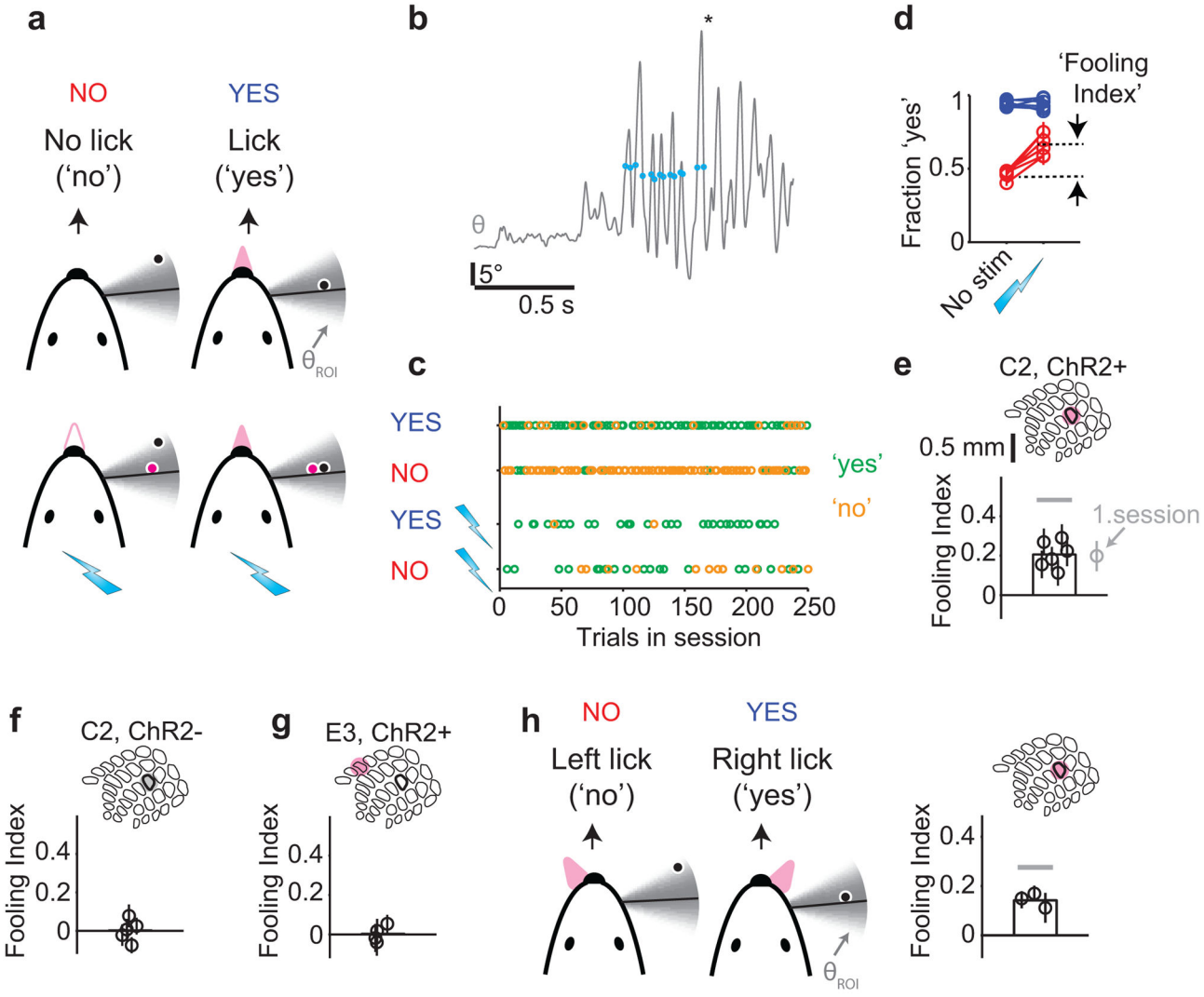

Figure 5. Closed-loop photostimulation causes illusory perception of object location

a. Four trial types during a photostimulation behavior session, depending on pole location and photostimulation (cyan lightning bolts). The virtual pole (magenta) was in the θ_{ROI}. Mice reported object location by licking or not licking.

b. Photostimulation (blue circles) coupled to whisker movement (grey, θ) during object location discrimination. Asterisk, answer lick.

c. Responses in the four trial types across one behavioral session. Green, 'yes' responses; yellow, 'no' responses.

d. Photostimulation on NO trials (red) in the C2 barrel increases the fraction of yes responses. Blue, YES trials. Error bars, SEM. Lines show individual mice.

e. Fooling Index (defined in d). Black circles, individual mice. Grey circle, first session, averaged across all mice. Error bars, SEM. Grey bar, mean maximum possible Fooling Index.

f. Same experiment as in a–e, without ChR2 expression.

g. Same experiment as in a–e, with ChR2 expression and photostimulation in the E3 barrel.

h. Symmetric response task; both object locations were indicated by licking at one of two lickports (lick left/lick right). Black circles, individual mice. Grey bar, mean maximum possible Fooling Index. Performance of each mouse is different from zero by one-tailed permutation test.

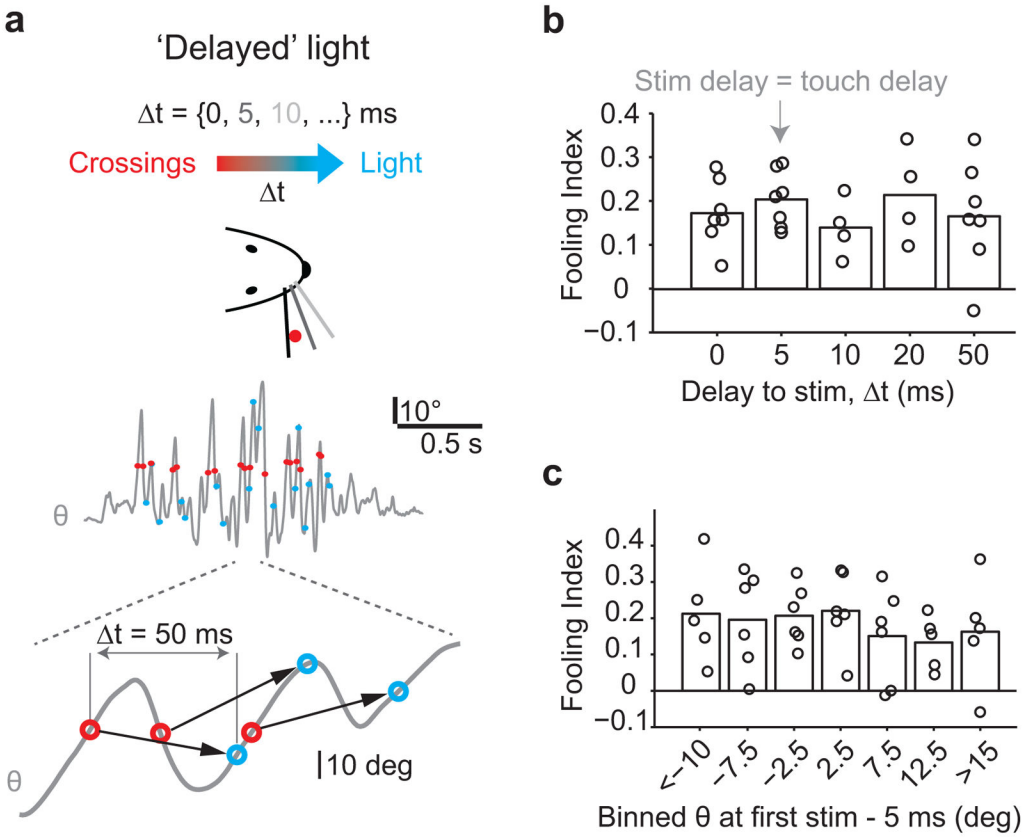

Figure 6. Millisecond time scale precise spike latencies are not required for detecting an object at a particular location

a. Top, 'Delayed' photostimulation of L4 neurons was triggered by whisker crossings with varying delays (Δ*t*). Bottom, whisker movements with whisker crossings (red circles) and corresponding photostimuli (cyan circles) for Δ*t* = 50 ms.

b. Fooling Index as a function of the delay between whisker crossing and photostimulation.

c. Fooling Index as a function of azimuthal angle at the time of stimulation.

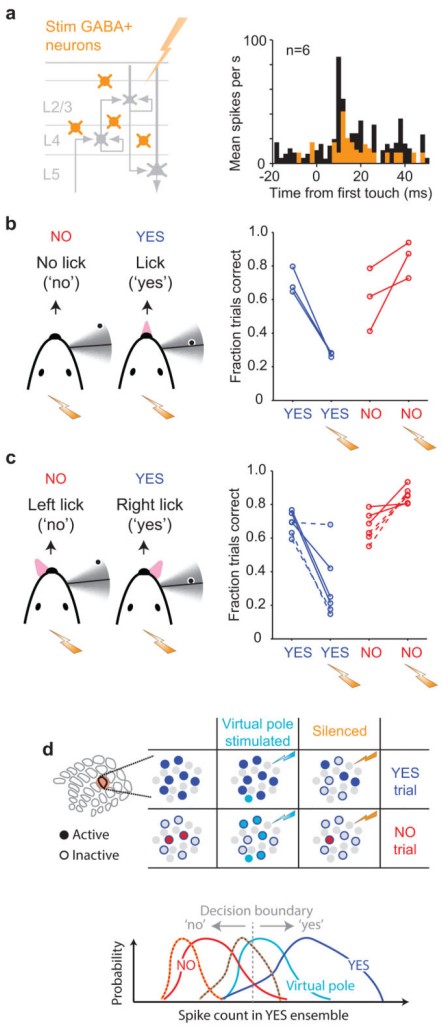

Figure 7. Optogenetic silencing of the C2 column biases behavioral choice toward 'no' responses, consistent with spike count coding

a. Left, silencing the C2 cortical column using ChR2-based stimulation of GABAergic neurons. Right, recordings from putative excitatory neurons under control (black) and photostimulation (yellow) conditions (peristimulus time histogram aligned to first touch; bin size, 2 ms; n = 6 neurons from 4 mice; Methods). The photostimulus (1.4 mW) began approximately 200 ms before first touch.

b. Reducing spike count in the C2 column reduces performance on YES trials, and improves performance on NO trials. Lines, 3 individual mice.

c. Same as b, for a symmetric response version of the object location discrimination task. Lines show data from 3 individual mice, for two photostimulation conditions with 2 mW average power (continuous illumination, dashed lines; illumination with 1 ms pulses at 80 Hz, same average power, solid lines).

d. We speculate that mice monitor spike count within the ensemble of L4 neurons in the C2 column normally activated by contact on YES trials (blue 'neurons', upper left corner of the table). The table shows a schematic of the L4 ensemble under the conditions tested in this study (Fig. 5–7). For example, on NO trials, a distinct but overlapping ensemble is activated

(red 'neurons'; the YES trial ensemble is indicated with blue outlines). On photostimulated NO (i.e. virtual pole; cyan) trials, activity is evoked in a subset of the YES ensemble, fooling mice into making 'yes' responses. Bottom, hypothetical distribution of decision variable (spike count in YES ensemble) used by mice to decide between a 'yes' and a 'no' response. Red, NO trials; blue, YES; cyan, NO with virtual pole and photostimulation (Fig. 5, 6); yellow dashed lines, silencing. If spike count in the YES ensemble of neurons exceeds a threshold value (the 'decision boundary'), the mouse makes a 'yes' response; otherwise the mouse makes a 'no' response.

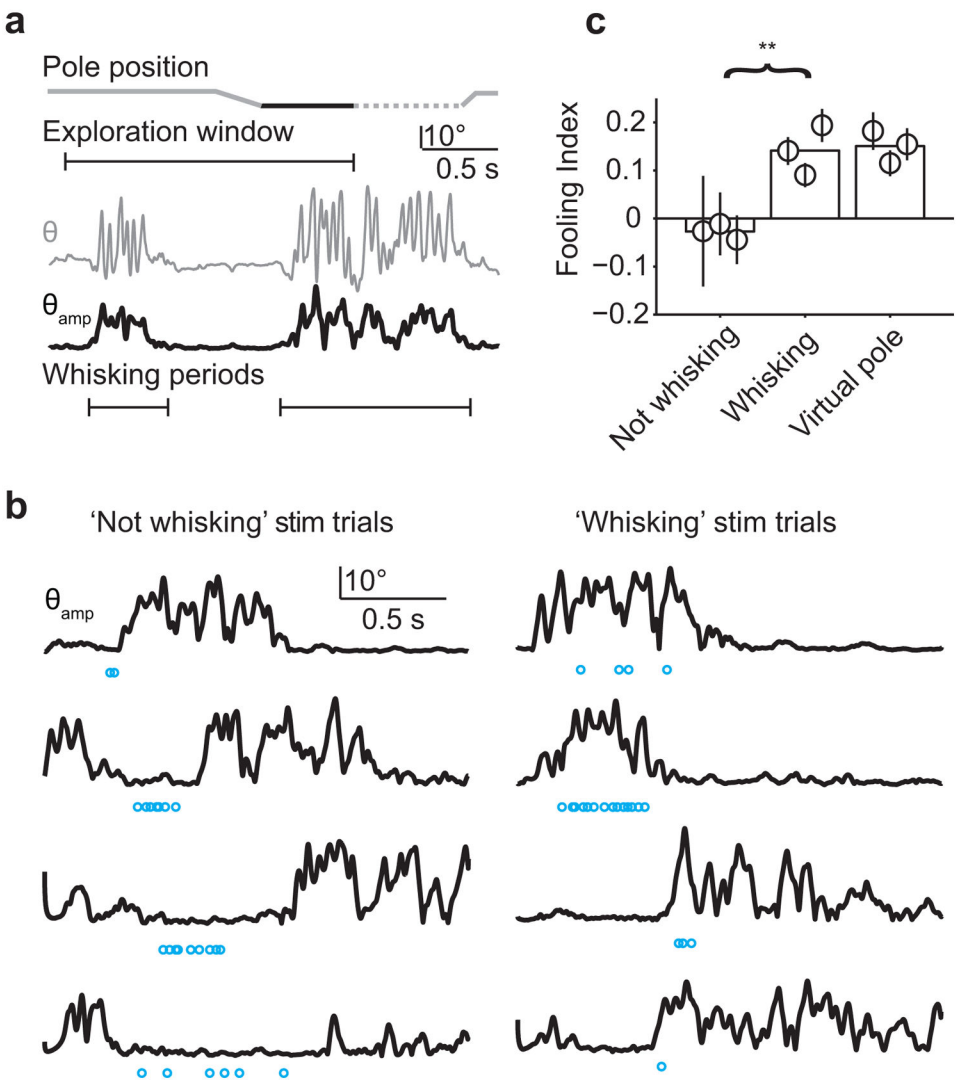

Figure 8. Illusory object location can only be evoked during periods of tactile exploration marked by whisking bouts

a. Example of whisking bouts in relation to trial start and pole motion. Whisker movement (θ, grey) and whisking amplitude (θ_{amp}, black).

b. Eight example trials, showing the time course of whisking (θ_{amp}, black) and the corresponding photostimulation pattern (cyan circles). Left, trials in which photostimulation occurred during periods without whisking. Right, trials in which photostimulation occurred during whisking.

c. Fooling Index for 'whisking' and 'not whisking' trials. Also plotted are interleaved standard virtual pole trials (Δt = 5 ms; as in Fig. 5e). Error bars, SEM.